context for understanding spatio-temporal patterns of tundra productivity and are available from the same satellite sensors that record NDVI for the GIMMS-3g dataset. We summarize the land surface temperature observations as the Summer Warmth Index (SWI), the sum of mean monthly temperatures for all months with mean temperatures above freezing (>0°C). The 2019 growing season was the warmest in the entire record; the mean SWI for the full circumpolar region (39.0°C-months) broke the previous record set in 2016 (34.9°C-months). The tundra regions of both continents experienced record warmth (section 5b). The 2019 SWI exceeded previous highs set in North America and Eurasia in 1994 and 2016, respectively. This warmth was not, however, accompanied by strong increases in NDVI, possibly due to lag effects arising from the below-normal summer temperatures experienced in 2018. Within the 38-year record, MaxNDVI values for 2019 ranked 19th, 9th, and 26th for the circumpolar Arctic, Eurasian Arctic, and North American Arctic, respectively. TI-NDVI values ranked 31st, 26th, and 35th for the circumpolar Arctic, Eurasian Arctic, and North American Arctic respectively.

j. Ozone and UV radiation—G. Bernhard., V. Fioletov, J.-U. Grooß, I. Ialongo, B. Johnsen, K. Lakkala, G. Manney, and R. Müller

Past emissions of chlorine-containing substances, such as chlorofluorocarbons (CFCs), have substantially contributed to the chemical destruction of ozone in the atmosphere (WMO 2018). The resulting ozone loss has led to increased ultraviolet (UV) radiation with adverse effects on human health and Earth's environment (EEAP 2019). The chemical destruction of polar ozone occurs within a cold low-pressure system (i.e., cyclone) known as the polar vortex, which forms over the North Pole every year during winter and spring (WMO 2018). Hence, the period of December 2018–April 2019 is emphasized in this report. As explained in more detail below, unusual conditions during this period enabled ozone concentrations in February and early March 2019 to reach the highest values in at least the past 15 years of satellite observations. In March 2019, the minimum Arctic daily total ozone column (TOC; i.e., ozone amounts integrated from the surface to the top of the atmosphere) was the highest value since 1988, for years when a well-defined polar vortex existed in March. With some exceptions, UV index (UVI) anomalies during this period were generally within the typical range of variability.

1) Ozone

Chemical processes that drive ozone depletion in the polar stratosphere are initiated at temperatures below about 195 K (–78°C) at altitudes of approximately 15 to 25 km. These low temperatures lead to the formation of polar stratospheric clouds (PSCs), which act as a catalyst to transform inactive forms of chlorine-containing substances to active, ozone-destroying chlorine species. At the beginning of December 2018, temperatures in the lower Arctic stratosphere dropped below the threshold for PSC formation and remained below this threshold and near the mean of the observational record (1979–2017) during the first three weeks of December. On 2 January 2019, a major sudden stratospheric warming (SSW) occurred, which led to a rapid rise of polar stratospheric temperatures over the course of a few days. During this event, the polar vortex split into three "offspring" vortices. As a result, stratospheric temperatures rose above the threshold for PSCs and remained well above this threshold for the remainder of the winter. The offspring vortices recombined in early March such that the polar vortex observed on 12 March was the strongest of the winter/spring 2018/19 period (Lee and Butler 2020). However, stratospheric temperatures at this time were too high for PSC formation.

Because of the early SSW event, chemical destruction of ozone was unusually low over the winter/spring period of 2018/19, as is confirmed by satellite-based observations. Measurements by the Microwave Limb Sounder (MLS) show that chlorine activation started in mid-December, resulting in a small decline in ozone concentrations, as expressed by the ozone mixing ratio (Fig. 5.28). Chlorine deactivation began in early January 2019 and was complete by late that month—consequently no chemical

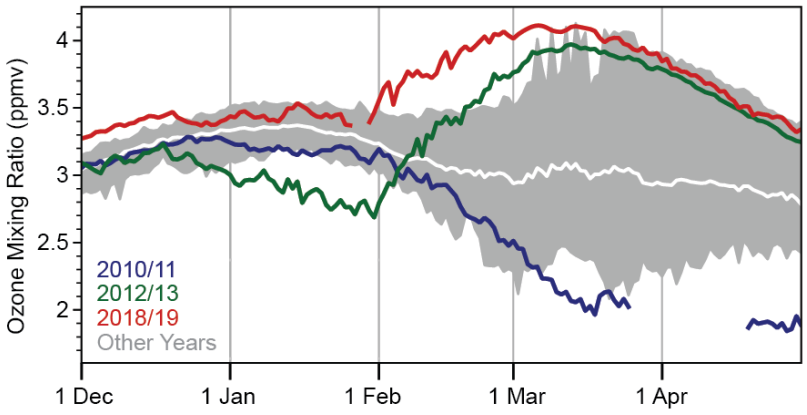

Fig. 5.28. Average ozone mixing ratios (ppmv) at an altitude of ~18 km for the area bounded by the polar vortex, as measured by *Aura* MLS. Data from 2018/19 (red), 2012/13 (green), and 2010/11 (blue) are compared with the average (solid white) and minimum/maximum range (gray shading) from 2004/05 to 2017/18, excluding 2010/11, 2012/13, and 2018/19. Gaps in the record for 2010/11 and 2018/19 are due to missing data.

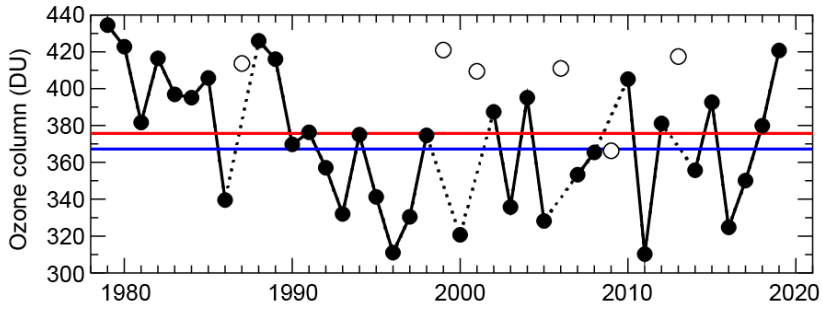

Fig. 5.29. Minimum of the daily average column ozone for Mar poleward of 63°N equivalent latitude (Butchart and Remsberg 1986). Open circles represent years in which the polar vortex was not well-defined in Mar, resulting in relatively high values due to mixing with lower latitude air masses and a lack of significant chemical ozone depletion. Red and blue lines indicate the average TOC for 1979–2018 and 2005–18, respectively. Ozone data for 1979–2016 are based on the combined total column ozone database version 3.4 produced by Bodeker Scientific (www.bodeker-scientific.com/data/total-column-ozone). Ozone data for 2017–19 are from the OMI. The graph is adapted from Müller et al. (2008) and WMO (2018), updated using ERA-Interim reanalysis data (Dee et al. 2011) for determining equivalent latitude.

ozone loss occurred after about mid-January. This sequence of conditions enabled ozone concentrations in February and early March 2019 to reach the highest values in at least the past 15 years, the period of the MLS observational record. The conditions in 2018/19 were similar to those in 2012/13 (Manney et al. 2015), although the strong SSW started a few days earlier in 2019 (Fig. 5.28). Unlike December 2018, December 2012 temperatures in the lower Arctic stratosphere were unusually cold, resulting in greater chlorine activation and much larger ozone loss in 2012/13 compared to 2018/19. The largest chemical ozone loss observed to date occurred in the winter of 2010/11 and was associated with an unusually prolonged cold period lasting through early April 2011, with temperatures in the lower stratosphere remaining low enough for PSC formation (Manney et al. 2011).

The evolution of Arctic TOC in March 2019 is compared to the satellite-derived observational record (1979–2018) in Fig. 5.29 using the minimum of the daily averages for March. March TOC is evaluated because chemically-induced Arctic ozone loss has the largest variability in this month (Fig. 5.28; WMO 2018). In March 2019, the minimum Arctic daily TOC was 421 Dobson units (DU), which was the highest value since 1988 for years when a well-defined polar vortex existed in March. The value was 12.0% (45 DU) above the average of the observational record (376 DU) and 14.6% (54 DU) above the average when MLS data are available (2005–18).

Spatial deviations of monthly average TOCs from historical (2005–18) averages (Figs. 5.30a,b) were estimated from the Ozone Monitoring Instrument (OMI; co-located with MLS on the *Aura* satellite) measurements. With the exception of an area centered over northwestern Canada, TOCs in March 2019 were above the mean over sunlit regions of the Arctic (Fig. 5.30a), consistent with the high ozone concentrations inside the lower stratospheric polar vortex during March 2019 (Fig. 5.28). These anomalies ranged between 0% over Scandinavia to 12% over Siberia. In mid-April, TOC departures exhibited a distinct geographical pattern with positive anomalies of up to 17% over Canada, the North Pole, and Siberia, and negative anomalies as large as –17% over Scandinavia and the North Sea (Fig. 5.30b).

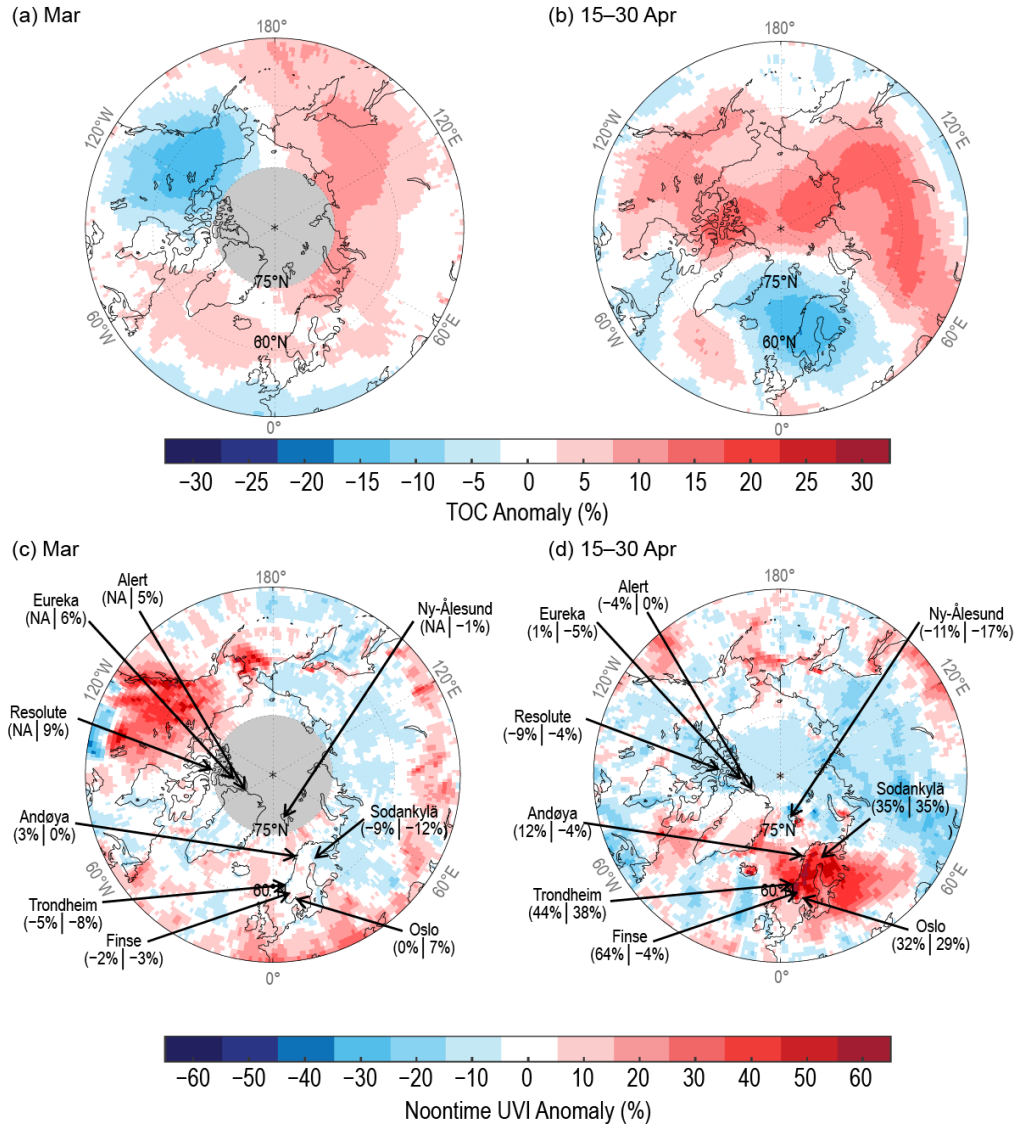

Fig. 5.30. Anomalies of TOC (%) for (a) Mar and (b) 15–30 Apr 2019. Anomalies of noontime UVI (%) for (c) Mar and (d) 15–30 Apr 2019. Anomalies are relative to 2005–18 averages. Maps are based on the OMTO3 Level 3 total ozone product (Bhartia and Wellemeyer 2002). (c) and (d) also compare UVI anomalies from OMI (first value in parenthesis) with ground-based measurements at nine locations (second value). Gray, solid circles centered at the North Pole indicate the areas where no OMI data are available due to the lack of sunlight at this time of year.

2) Ultraviolet radiation

UV radiation is quantified with the UVI, which is a measure of the capacity of UV radiation to cause erythema (sunburn) in human skin (WHO 2002). In addition to its dependence on TOC, the UVI depends on the sun angle, clouds, and surface albedo (Weatherhead et al. 2005). In the Arctic, the UVI scale ranges from 0 to about 7, with the smallest annual peak radiation levels (UVI values < 4) observed at sites closest to the North Pole. UVI values ≤ 5 indicate low-to-moderate risk of erythema (WHO 2002).

UVI anomalies are assessed using both OMI and ground-based measurements, with the former providing better spatial coverage and the latter providing greater regional accuracy (Bernhard et al. 2015). Figures 5.30c,d quantify the spatial differences in monthly average noontime UVIs from historical (2005–18) averages based on measurements by OMI and by ground-based instruments at nine research stations located in the Arctic and Scandinavia. Areas with high UVIs roughly match areas with low TOCs and vice versa, but UVI anomalies have larger spatial variability because of their added dependence on clouds. In the following discussion, we emphasize

March 2019 and 15–30 April 2019. During the latter period, unusually large UVI anomalies over the Nordic countries occurred, while ozone and UVI anomalies for other months were generally within the typical range of variability.

In March 2019, monthly average noontime UVIs calculated from OMI observations over northwestern Canada were up to 55% above the 2005–18 mean (Fig. 5.30c). This region of unusually high UVIs coincided with the area of low TOCs in Fig. 5.30a. Large UVI anomalies of up to 50% were also observed west of Alaska. UVI anomalies for the remainder of the Arctic computed from OMI and ground-based measurements were below 15%. Because of the low solar zenith angle in March, absolute anomalies did not exceed 1.9 UVI units for latitudes higher than 60°N.

During the period of 15–30 April, a persistent high-pressure system was centered over the Nordic countries, and the ensuing periods of clear skies contributed to large UVI anomalies of up to 65% (Fig. 5.30d). Anomalies calculated from OMI and ground-based data agreed to within ±8% at almost all locations. Exceptions included Andøya and Finse due to local weather (cloudiness) and ground conditions (low albedo due to unusually wet snow cover), respectively. The influence of local conditions creates inconsistencies between satellite and ground-based measurements and illustrates the limitations of estimating UV radiation from space. These inconsistencies are largest at locations that are either affected by variable conditions within the satellite instrument's field of view (cloudiness, albedo, topography) or differences between the actual surface albedo and the albedo climatology used by OMI (Tanskanen et al. 2004).

Acknowledgments

The editors thank Dr. Martin Jeffries, USACE Cold Regions Research and Engineering Laboratory, and Florence Fetterer, National Snow and Ice Data Center, for providing an initial review of the full chapter. Their careful read and thoughtful input improved each of the sections and, importantly, led to better coherency between the sections.

a. Overview

- Jackie Richter-Menge appreciates support from NOAA's Arctic Research Office.
- Matthew Druckenmiller was supported by the Study of Environmental Arctic Change (SEARCH, NSF grant PLR-1331100).

b. Surface air temperature

- Jim Overland has support from the NOAA Arctic Research Program.
- Tom Ballinger acknowledges support from the Experimental Arctic Prediction Initiative at the University of Alaska Fairbanks.

d. Sea ice

Walt Meier's contribution was supported by the NASA Snow and Ice Distributed Active Archive Center (DAAC) at NSIDC, part of the NASA Earth Science Data and Information System (ESDIS) Project.

e. Greenland ice sheet

Macro Tedesco acknowledges financial support by the National Science Foundation (PLR-1603331, PLR-1713072), NASA (NNX17AH04G, 80NSSC17K0351) and the Heising-Simons Foundation. Financial support for measurements along the K-transect has been received from the Dutch Polar Program of NWO. Data from the Programme for Monitoring of the Greenland Ice Sheet (PROMICE) and the Greenland Analogue Project (GAP) were provided by the Geological Survey of Denmark and Greenland (GEUS) at http://www.promice.dk. Computational resources for running the MAR model have been provided by the Consortium des Équipements de Calcul Intensif (CÉCI), funded by the Fonds de la Recherche Scientifique de Belgique (F.R.S.FNRS) under grant no. 2.5020.11 and the Tier-1 supercomputer (Zenobe) of the Fédération Wallonie Bruxelles infrastructure funded by the Wallonia region under grant agreement no. 1117545.

j. Ozone and UV Radiation

Germar Bernhard and coauthors acknowledge the support of Biospherical Instruments, San Diego; the Research Council of Norway through its Centers of Excellence funding scheme, project number 223268/F50; the Academy of Finland for supporting UV measurements through the FARPOCC and SAARA projects; the European Space Agency for supporting the DACES project; and the European Union for supporting e-shape. We also thank the Microwave Limb Sounder team at NASA's Jet Propulsion Laboratory for data processing and analysis support; Tove Svendby from the Norwegian Institute for Air Research and Arne Dahlback from the University of Oslo for overseeing UV measurements at Oslo, Andøya, and Ny-Ålesund; and Juha M. Karhu, Tomi Karppinen, and Markku Ahponen from the Finnish Meteorological Institute for operating the Brewer UV spectroradiometer at Sodankylä.

Sidebar 5.1. Shifting fish distributions in the Bering Sea

We'd like to thank the scientists and crews who took part in these long-term groundfish surveys in the eastern and northern Bering Sea. We also thank R. Haehn for pulling the 2019 survey data.

Sidebar 5.2 Permafrost carbon

Support provided by:

- NSF Research, Synthesis, and Knowledge Transfer in a Changing Arctic: Science Support for the Study of Environmental Arctic Change (SEARCH) Grant # 1331083. (2014-2020)
- NSF PLR Arctic System Science Research Networking Activities (RNA) Permafrost Carbon Network: Synthesizing Flux Observations for Benchmarking Model Projections of Permafrost Carbon Exchange (2019-2023).